Journal of Physics:
Condensed Matter

PURPOSE-LED PUBLISHING™

PAPER

A new interlayer potential for hexagonal boron nitride

To cite this article: Tolga Akıner *et al* 2016 *J. Phys.: Condens. Matter* **28** 385401

View the article online for updates and enhancements.

You may also like

- Understanding thermal transport in asymmetric layer hexagonal boron nitride heterostructure
Jingchao Zhang, Xinyu Wang, Yang Hong et al.
- Thermal conductivity of h-BN monolayers using machine learning interatomic potential
Yixuan Zhang, Chen Shen, Teng Long et al.
- The role of flexural coupling in heat dissipation from a two-dimensional layered material to its hexagonal boron nitride substrate
Zhun-Yong Ong, Gang Zhang and Yong-Wei Zhang

This content was downloaded from IP address 144.122.201.61 on 03/10/2026 at 19:16

IOP Publishing Journal of Physics: Condensed Matter
J. Phys.: Condens. Matter **28** (2016) 385401 (8pp) doi:10.1088/0953-8984/28/38/385401

A new interlayer potential for hexagonal boron nitride

Tolga Akıner, Jeremy K Mason and Hakan Ertürk

Department of Mechanical Engineering, Boğaziçi University, Istanbul, Turkey

E-mail: hakan.erturk@boun.edu.tr

Received 24 March 2016, revised 15 June 2016
Accepted for publication 20 June 2016
Published 25 July 2016



Abstract

A new interlayer potential is developed for interlayer interactions of hexagonal boron nitride sheets, and its performance is compared with other potentials in the literature using molecular dynamics simulations. The proposed potential contains Coulombic and Lennard-Jones 6–12 terms, and is calibrated with recent experimental data including the hexagonal boron nitride interlayer distance and elastic constants. The potentials are evaluated by comparing the experimental and simulated values of interlayer distance, density, elastic constants, and thermal conductivity using non-equilibrium molecular dynamics. The proposed potential is found to be in reasonable agreement with experiments, and improves on earlier potentials in several respects. Simulated thermal conductivity values as a function of the number of layers and of temperature suggest that the proposed LJ 6–12 potential has the ability to predict some phonon behaviour during heat transport in the out-of-plane direction.

Keywords: interlayer potential, hexagonal boron nitride, molecular dynamics, potential parameterization, orthotropic material

(Some figures may appear in colour only in the online journal)

1. Introduction

The properties of low dimensional materials often differ significantly from those of their bulk counterparts, and offer promising opportunities for novel devices and applications. Current advanced materials research aims to develop new material components or designs that benefit from the improved properties of low dimensional materials. For hexagonal boron nitride (hBN), improved properties include superior stability, high chemical resistance, hardness, mechanical strength and thermal conductivity [1, 2]. Moreover, hBN is distinguished as an electrical insulator, and has been used as a high temperature lubricant, a substrate or heat sink for electronic devices, and in ceramic production and coatings [3]. Structurally, hBN is a low dimensional material with a honeycomb lattice of alternating boron and nitrogen atoms in plane (figure 1(a)), and with layers stacked with an AB stacking arrangement out of plane (figure 1(b)). Visuals are created using VMD software [4].

Studies concerning hBN are more limited than those on similar materials such as graphene, and further characterization of hBN and understanding the physical behaviour is required. Moreover, there are inconsistincies in the available data. As an example, experiments show that the measured thermal conductivity depends on the synthesis method, measurement technique, and sample size. In-plane measured thermal conductivities of about 11.7 nm and 13.3 nm thick samples were reported to be 150 W $m^{-1}K^{-1}$ and 225 W $m^{-1}K^{-1}$ at 300 K, respectively [5], whereas the measured thermal conductivities of 5-layer and 11-layer samples were reported to be 250 W $m^{-1}K^{-1}$ and 360 W $m^{-1}K^{-1}$ at 300 K, respectively [6].

Molecular dynamics (MD) simulations offer the ability to investigate material properties in the absence of experimental complications to help identify physical behaviours. However, accurate representation of the system requires suitable interatomic potentials. This has been done extensively for materials such as graphene [7–9], but the number of studies for hBN is limited. While mechanical and thermal properties such as the bending and tensile rigidity, Poisson's ratio, heat capacity, and thermal expansion coefficient [10, 11] are considered, many of these properties can not be characterized accurately or precisely. Notably, the thermal conductivity of hBN in MD simulations is reported to be anywhere from 80 W $m^{-1}K^{-1}$ to 1000 W $m^{-1}K^{-1}$ [12, 13].

© 2016 IOP Publishing Ltd Printed in the UK
All rights, including for text and data mining, AI training, and similar technologies, are reserved.

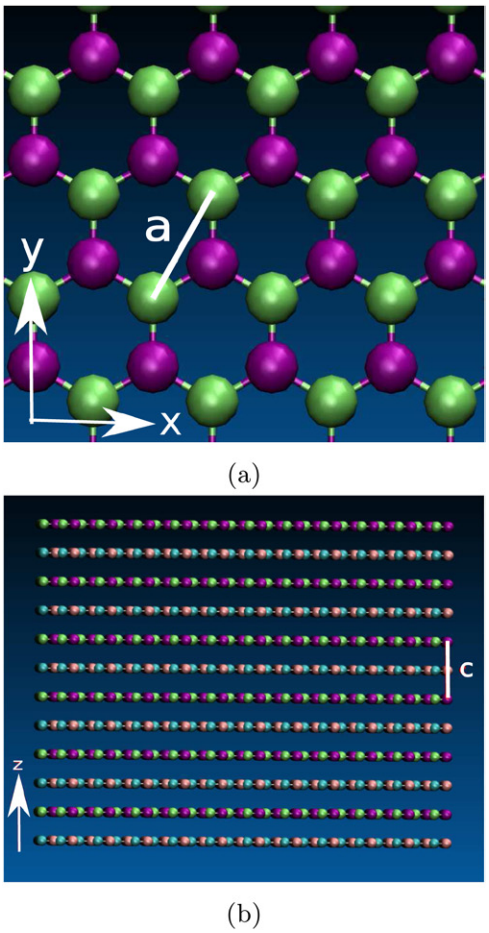


Figure 1. The (a) in-plane and (b) out-of-plane atomic structure of MLhBN.

The existing MD simulations only examine the in-plane properties of hBN, and most consider just a single hBN sheet even though hBN is usually multi-layered in practice [1, 5, 6]. This is significant because multi-layered hBN (MLhBN) has thermal and mechanical properties that differ by orders of magnitude along the in-plane and out-of-plane directions. Experiments on 50–120 μm thick hBN samples found the in-plane elastic constant c_{11} and out-of-plane elastic constant c_{33} to be 811 GPa and 27 GPa, respectively [14]. Similarly, experiments found the thermal conductivity at 300 K to be 250 W $m^{-1}K^{-1}$ and 2 W $m^{-1}K^{-1}$ in the in-plane and out-of-plane directions, respectively [15].

Since the accuracy of MD simulations is limited by the interatomic potentials used, the interatomic potential should be able to accurately reproduce relevant behaviors at the nano-scales. In the case of thermal properties, this includes collective motions such as phonon transport [16, 17]. There are just a few studies in the literature with interatomic potentials which are capable of characterizing the anisotropic behaviour accurately, and our objective is to improve on them.

The structure of hBN naturally suggests that the in-plane and out-of-plane atomic bonding be handled differently. The Tersoff potential [18] is commonly used for the covalent in-plane interactions between adjacent borons and nitrogens. Originally developed for Si-Ge and C-Si systems, the potential was eventually extended to hBN [19] and is now used extensively in the literature [12, 13, 20]. The out-of-plane interactions appear to be mainly governed by Coulombic forces, dispersion forces and Pauli repulsion, meaning that it would not be appropriate to use the Tersoff potential for interlayer bonding and a different potential should be used. Lindsay and Broido [20] neglected Coulombic forces and assumed same Lennard-Jones (LJ) 6–12 parameters for all of the B–B, N–N and B–N interactions in a recent study, but this contradicts density functional theory (DFT) calculations that showed that the Coulombic forces play a critical part in stabilizing the stacking mode and regulating interlayer sliding corrugation [21]. Leven *et al* [22] developed a potential for the interlayer interactions based on extensive DFT simulations. However, this function is computationally expensive for sizable MD simulations, and potentials calibrated to DFT results do not necessarily give physically reasonable behaviour at finite temperatures [23]. Green *et al* [24] proposed a LJ 6–12 potential with a Coulombic term, with the potential parameters and resulting elastic constants are calculated theoretically. Since there were few experiments available at that time, they were able to compare their results only for c_{33} and did not test the potential performance for other properties. Kuzuba *et al* [25] adopted a similar approach using the same functional form, but derived the potential parameters from the experimental structure and elastic constants of MLhBN. However, the derivations of these potentials included some questionable assumptions such as same parameters for different type of atomic interactions, and used only the limited experimental data that was available at that time.

The objective of this study is to derive a computationally efficient and easy to implement potential that is capable of reproducing the thermo-physical properties of hBN accurately, using MD simulations. More recent experimental data is used to improve the accuracy of existing potentials and a comparison of the potential with other potentials in the literature is also presented.

2. Methodology

2.1. Potential function parameters: derivation

The calculation follows a similar procedure to that of Kuzuba *et al* [25]. Let $\phi_{ij}(r_{ij})$ be the interaction energy between the ith and jth atoms in two distinct layers and separated by a distance

$$r_{ij} = \sqrt{(x_i - x_j)^2 + (y_i - y_j)^2 + (z_i - z_j)^2} \tag{1}$$

where the layers are parallel to the x-y plane. The interlayer interaction energy of the infinite crystal is then

$$E = \frac{1}{2} \sum_m \sum_{n \neq m} \sum_{i \in L_m} \sum_{j \in L_n} \phi_{ij}(r_{ij}) \tag{2}$$

where m and n are integer labels for the layers and L_m and L_n are the set of integer labels for the atoms in layer m and n, respectively. The contribution to the interaction energy of a single pair of B and N atoms in layer zero (the reference layer) is then

$$E = \frac{1}{2}\sum_{n\neq 0}\sum_{j\in L_n}\phi_{\mathrm{B}j}(r_{\mathrm{B}j}) + \phi_{\mathrm{N}j}(r_{\mathrm{N}j}) \tag{3}$$

where $\phi_{\mathrm{B}j}$ and $\phi_{\mathrm{N}j}$ are the potentials between the pair of atoms in the reference layer and atom j. The function defined by equation (3) has attractive, repulsive and electrostatic components. The repulsive and attractive terms are assumed to be of the LJ 6–12 type, and Coulomb's law is used for the electrostatic interactions. This yields

$$\varphi_{\mathrm{B}j}(r_{ij}) = -\alpha_{\mathrm{B}j}r_{\mathrm{B}j}^{-6} + \beta_{\mathrm{B}j}r_{\mathrm{B}j}^{-12} + K_{\mathrm{C}}q_{\mathrm{B}}q_j r_{\mathrm{B}j}^{-1} \tag{4a}$$

$$\varphi_{\mathrm{N}j}(r_{ij}) = -\alpha_{\mathrm{N}j}r_{\mathrm{N}j}^{-6} + \beta_{\mathrm{N}j}r_{\mathrm{N}j}^{-12} + K_{\mathrm{C}}q_{N}q_j r_{\mathrm{N}j}^{-1} \tag{4b}$$

where the coefficients $\alpha_{\mathrm{B}j}$, $\alpha_{\mathrm{N}j}$ and $\beta_{\mathrm{B}j}$, $\beta_{\mathrm{N}j}$ are assumed to be positive and control the strength of the attractive and repulsive interactions, q is the atomic partial charge in units of the elementary charge, and K_{C} is the Coulombic constant. Since charge balance requires that the partial charges of the B and N atoms have same magnitude, the three different interactions (B–B, N–N, B–N) lead to the seven unknowns; α_{NN}, α_{BB}, α_{BN}, β_{NN}, β_{BB}, β_{BN} and q. This implies that at least seven constraint equations are required to solve for the parameters of the interlayer potential of MLhBN. The Van der Waals radius for B is 192 pm [26], much smaller than the 330 pm between hBN layers. Neglecting the short range B–B interactions, as is often done for ionic materials [27], reduces the number of unknowns to five. Since N has a nonbonding electron orbital that extends above and below the layer [28], the N–N and B–N interactions cannot similarly be neglected. If equations (4*a*) and (4*b*) are inserted into equation (3) with this simplification, the interlayer contribution of the reference pair becomes:

$$\begin{aligned} E = &-\frac{1}{2}\alpha_{\mathrm{B}j}\sum_{n\neq 0}\sum_{j\in L_n} r_{\mathrm{B}j}^{-6} + \frac{1}{2}\beta_{\mathrm{B}j}\sum_{n\neq 0}\sum_{j\in L_n} r_{\mathrm{B}j}^{-12} \\ &+ \frac{K_{\mathrm{C}}}{2}q_B q_j \sum_{n\neq 0}\sum_{j\in L_n} r_{\mathrm{B}j}^{-1} - \frac{1}{2}\alpha_{\mathrm{N}j}\sum_{n\neq 0}\sum_{j\in L_n} r_{\mathrm{N}j}^{-6} \\ &+ \frac{1}{2}\beta_{\mathrm{N}j}\sum_{n\neq 0}\sum_{j\in L_n} r_{\mathrm{N}j}^{-12} + \frac{K_{\mathrm{C}}}{2}q_N q_j \sum_{n\neq 0}\sum_{j\in L_n} r_{\mathrm{N}j}^{-1} \end{aligned} \tag{5}$$

The attractive and repulsive lattice summations in equation (5) can be evaluated term-by-term since the atomic positions in the ground state structure are known. It is observed that these summations converge with 400 hundred atoms in each layer, and the calculations are done for 900 hundred atoms in a layer.

The Coulombic contribution to the interaction energy is only conditionally convergent, preventing similar evaluation of these sums. The Ewald summation method is used instead, following a procedure described elsewhere [24, 25], to replace those with exponentially decaying sums over the in-plane reciprocal lattice vectors $\vec{g}$. This yields the energy due to electrostatic interactions as

$$E_c = K_{\mathrm{C}}q^2\frac{2\pi}{A}\sum_{\vec{g}}\cos(\vec{g}\cdot\vec{u})\exp(-|\vec{g}|d) \tag{6}$$

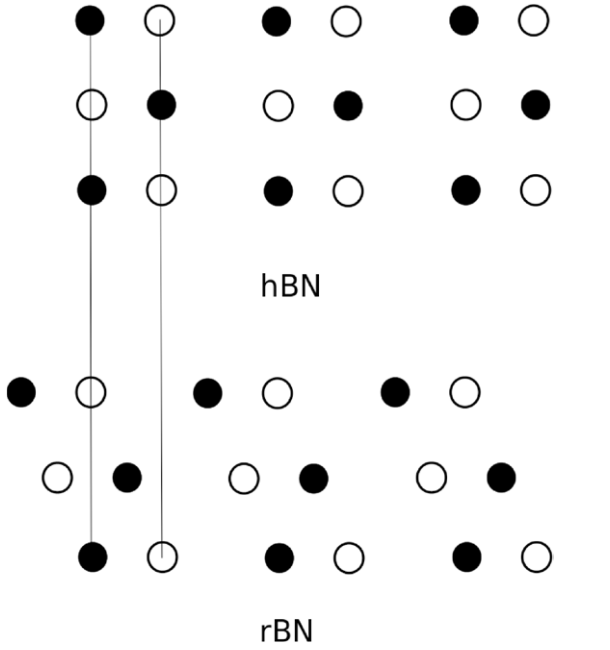


Figure 2. Schematic for hBN and bond shifted structure of rBN.

where A is the area of the real-space unit cell (0.0543 nm^2), $\vec{u}$ is the lateral shift of the layer relative to the reference layer, and d is the distance between neighboring layers. Equation (6) replaces the summations over r^{-1} in equation (5). As a result, the interlayer potential E can be defined as a function of five fitting parameters, together with $\vec{u}$ and d as determined by the structure. Constraints on this function include the DFT equilibrium layer separation, experimental c_{33} and c_{44} values, and the binding energy at equilibrium. This yields 4 constraints and 5 unknowns, leaving an undetermined system of equations. This is resolved by assuming that the potential function for rhombohedral boron nitride (rBN) is identical to hBN, differing only in the registration of neighbouring layers; the stacking of rBN shifts the third layer by one B–N bond length in the in-plane direction as shown in figure 2. The experimental equilibrium layer separation, c_{33} and c_{44} values, and binding energy at equilibrium for rBN provide four additional constraints. The experimental lattice parameters are reported as $a = 0.2506$ nm and $c = 0.6657$ nm (figure 1) for hBN [14], and $a = 0.2504$ nm and $c = 0.6667$ nm for rBN [29]. Since the derivation procedure effectively calibrates the potential for the 0 K structure, the experimental room temperature lattice constants are larger than the ideal because of thermal expansion. Therefore the interlayer distance, d, is taken to be 0.320 nm for hBN and 0.319 nm for rBN as predicted by DFT calculations considering 0 K [30]. The requirement that the potential be at a minimum at the equilibrium layer spacing yields two constraint equations, one for hBN and one for rBN:

$$\frac{\partial E}{\partial z} = \sum_{n\neq 0}\sum_{j\in L_n}\left.\frac{\partial\phi(r_{ij})}{\partial z_{ij}}\right|_{z_{ij}=\mathrm{nd}} = 0 \tag{7}$$

where z_{ij} is the z component of the atomic separation. The following four constraint equations are obtained by relating

Table 1. Target constraint equation values, the 0 K least square solution, and 300 K MD results.

	MD	Fitted	Target
$\frac{\partial E}{\partial z}$(kcal mole^{-1}K^{-1})	—	0	0
$\frac{\partial E}{\partial z}$(kcal mole^{-1}K^{-1})	—	0.3299	0
c_{33}^{hBN}(GPa)	29.9086	26.876	27 [14]
c_{33}^{rBN}(GPa)	—	28.5822	28.5 [29]
c_{44}^{hBN}(GPa)	5.1873	7.5855	7.7 [14]
c_{44}^{rBN}(GPa)	—	2.166	2.052 [29]
E_b^{hBN}(kcal mole^{-1})	−3.5949	−1.9332	−1.9063 [24]
E_b^{rBN}(kcal mole^{-1})	—	−1.8204	−1.8516 [24]

Table 2. Fitting parameters of the proposed study and others from the literature.

	This work	[24]	[25]
ϵ_{BN}(kcal mole^{-1})	0.007	0.0476	0.0872
ϵ_{NN}(kcal mole^{-1})	0.2496	0.0544	0.027
σ_{BN}(nm)	0.375	0.34 256	0.3137
σ_{NN}(nm)	0.31461	0.33 106	0.38 013
q (e)	1.1378	1.15	1.05

the experimental elastic constants to the second derivatives of equation (3).

$$\frac{\partial^2 E}{\partial z^2} = \sum_{n\neq 0}\sum_{j\in L_n} \frac{\partial^2 \phi(r_{ij})}{\partial z_{ij}^2}\bigg|_{z_{ij}=\mathrm{nd}} = \frac{c_{33}A}{d} \tag{8}$$

$$\frac{\partial^2 E}{\partial x^2} = \sum_{n\neq 0}\sum_{j\in L_n} \frac{\partial^2 \phi(r_{ij})}{\partial x_{ij}^2}\bigg|_{z_{ij}=\mathrm{nd}} = \frac{c_{44}A}{d} \tag{9}$$

Equations (8) and (9) are evaluated with the atoms in the 0 K equilibrium positions. Experimental elastic constants for hBN [14] and rBN [29] are evaluated for the room temperature equilibrium interlayer spacing in an attempt to handle thermal softening. The last two constraint equations simply equate equation (3) to an overall binding energy. The values of the elastic constants and theoretical binding energy per pair of atoms are taken from the literature, and are shown in table 1. The resulting overdetermined system is solved by least squares minimization to find the parameters reported in table 2 [31]. These are presented for the following type of LJ 6–12 function.

$$\phi_{\mathrm{LJ}}(r_{ij}) = 4\epsilon_{ij}\left[-\left(\frac{\sigma_{ij}}{r_{ij}}\right)^{-6} + \left(\frac{\sigma_{ij}}{r_{ij}}\right)^{-12}\right] + K_{\mathrm{C}} q_i q_j r_{ij}^{-1} \tag{10}$$

where K_{C} is Coulombic constant, σ, ϵ, and q are the potential parameters.

2.2. Performance of potential function: MD simulation details

MD simulations were used to evaluate the performance of the LJ 6–12 potential derived in section 2. An hBN model with 12 layers (shown in figure 1) ensured sufficient length in the z direction to allow the application of small strains without periodic boundary effects. The model was 5×4.7 nm^2 in plane, and included 10 560 atoms spaced according to the equilibrium spacing of hBN with periodic boundary conditions in all directions. The timestep was set to 1 fs, orders of magnitude smaller than the estimated phonon lifetime in transverse mode for hBN [20]. A standard Tersoff potential [19] was employed for the intralayer interactions, and the proposed LJ 6–12 potential from section 2.1 and two potentials from the literature [24, 25] (shown in table 2) were used for the interlayer interactions. Cutoff distances were set to 0.8 nm for the attractive and repulsive terms. The energy of the system was first minimized, then the temperature and pressure were equilibrated using the isothermal-isobaric ensemble (NPT) at specified temperature. All components of the stress tensor were independently set to 0 atm for 20 ps, at which point the system was observed to be in equilibrium. All MD calculations were caried out in LAMMPS [32].

2.2.1. Elastic constant calculations. After stabilization, the system was switched to the canonical ensemble (NVT) and the stress tensor was measured for 100 ps. The simulation box was then deformed, the system energy was minimized, and the stress tensor was averaged over 100 fs intervals in the deformed condition for an additional 100 ps. Note that the individual stress components must be controlled separately due to the orthotropy of MLhBN. Strain was applied in tension or compression in the z direction, or as a shear in the x direction on the z face. For sufficiently small strains, the elastic constants can be calculated as follows:

$$c_{33} = \frac{\sigma_{zz}^d - \sigma_{zz}^i}{\epsilon_{zz}} \tag{11}$$

$$c_{44} = \frac{\sigma_{xz}^d - \sigma_{xz}^i}{\gamma_{xz}} \tag{12}$$

where ϵ_{zz} and γ_{xz} are the imposed normal and shear strains, and the superscripts d and i respecively denote the deformed and initial stages for the stress component σ, respectively.

2.2.2. Thermal conductivity calculations. The same initial simulation conditions and equilibration procedure were used as for the elastic constant calculation, and the thermal conductivity of MLhBN in the out-of-plane direction was estimated using reverse non-equilibrium molecular dynamics (RNEMD) with the Muller–Plathe algorithm [33]. The simulation box was divided into 12 slabs along the out-of-plane direction with each slab containing one hBN sheet, and a heat flux was applied in this direction by exchanging the velocities of atoms in different slabs. Velocity swapping occured every 100 fs, with the two atoms with the highest velocities in one slab and

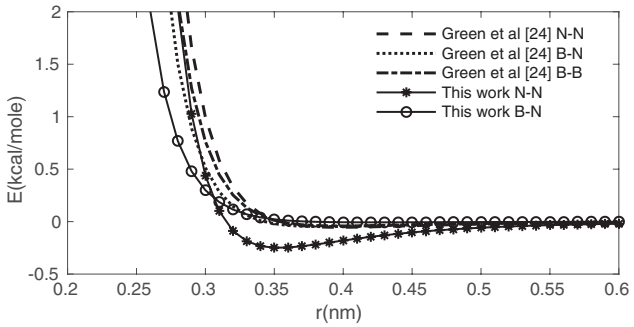


Figure 3. Potential energy versus interatomic distance for proposed LJ 6–12 potential (in the form of (10)) and Green *et al* [24].

the lowest velocities in the other being swapped. After NPT equilibration, the ensemble was switched to the microcanonical ensemble (NVE), a heat flux was applied to the system for 50 ps, and the temperature difference between the hot and cold slabs is measured for another 500 ps. The temperature of a slab is calculated with the formula

$$T = \frac{\sum m_i v_i^2}{3Nk_B} \tag{13}$$

where m_i is the mass, and v_i is the velocity of the ith atom, N is the number of atoms, and k_B is Boltzmann's constant. The temperature gradient was averaged over 100 fs intervals. We observed that the heat flux and temperature gradient had converged for the last 400 ps, meaning that the system had reached steady state. Once the heat flux and the temperature gradient were calculated, the thermal conductivity was estimated using Fourier's law:

$$k = \frac{q''}{\partial T/\partial z} \tag{14}$$

where q'' is heat flux per unit area and $\partial T/\partial z$ is the temperature gradient along the out-of-plane direction.

3. Results and discussion

3.1. Potential functions

The interatomic distance versus potential energy is shown for the derived potential and the potential offered by Green *et al* [24] in figure 3. The proposed potential has a noticeably higher binding energy for the N–N interaction.

3.2. Stability of the structure

The equilibrium interlayer spacing is calculated from MD simulations by averaging the distance between layers, and is presented for the derived potential and those of Green *et al* [24] and Kuzuba *et al* [25] in figure 4(a). Our potential deviates 2.25% from the experimental value of 0.33 nm, while the other potentials deviate by 3% and 6%, respectively. A corresponding trend is also observed for the density of MLhBN in figure 4(b), where the other potentials underestimate the density as compared to the proposed potential. It can be observed

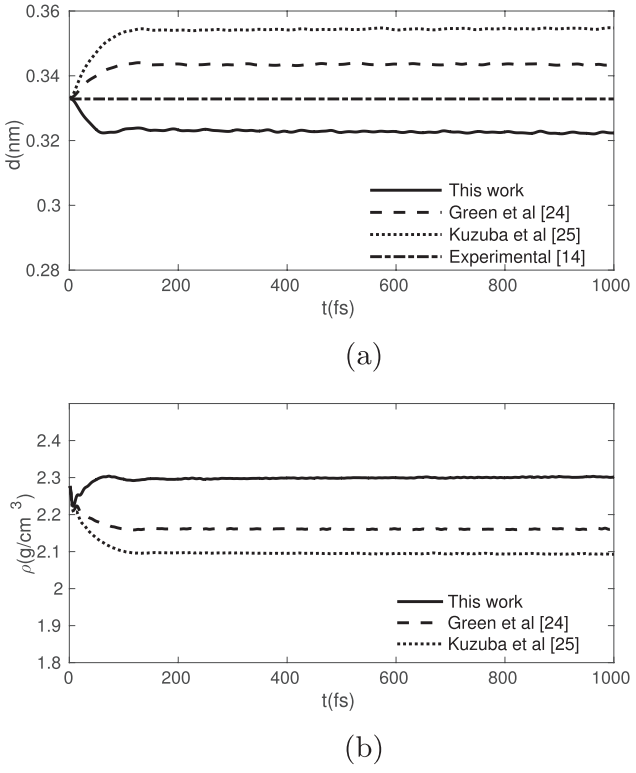


Figure 4. Layer spacing (a) and density (b) for MLhBN, calculated by MD simulations.

that the potentials in the literature overestimate the interlayer spacing while the derived potential slightly underestimates it.

3.3. Elastic constants

The temperature and pressure responses of the model with the proposed potential are shown in figure 5. The system is equilibrated for 100 ps and the components of the stress tensor are averaged over 100 fs intervals. Then the system is deformed and evolved for 200 ps, with 100 ps for the system to converge and 100 ps to average the stress components. Stress–strain plots for simulations and experiment [14] are presented in figure 6. The elastic constants c_{33} (in compression and tension), and c_{44} for three different strain values for each of the three interlayer potentials are also evaluated from stress–strain plots and compared with the experimental values in table 3. Figure 6(a) shows that the proposed LJ 6–12 potential parameters slightly overestimates the experimental c_{33} in compression, whereas the others slightly underestimate. However, MD results of the proposed LJ 6–12 potential is much closer to the experimental c_{33} in tension than the others as seen in figure 6(b). More precisely, a relative error of 11.5%, while those of Green *et al* [24] and Kuzuba *et al* [25] have relative errors of 28.6% and 41.4% as seen in table 3. The reason that c_{33} is higher in compression than tension is the asymmetry of the potential. The improved accuracy of the proposed LJ 6–12 potential, when compared to the other potentials can also be observed for c_{44} in figure 6(c).

The more accurate elastic constants suggest that the proposed LJ 6–12 will model transverse phonon modes more

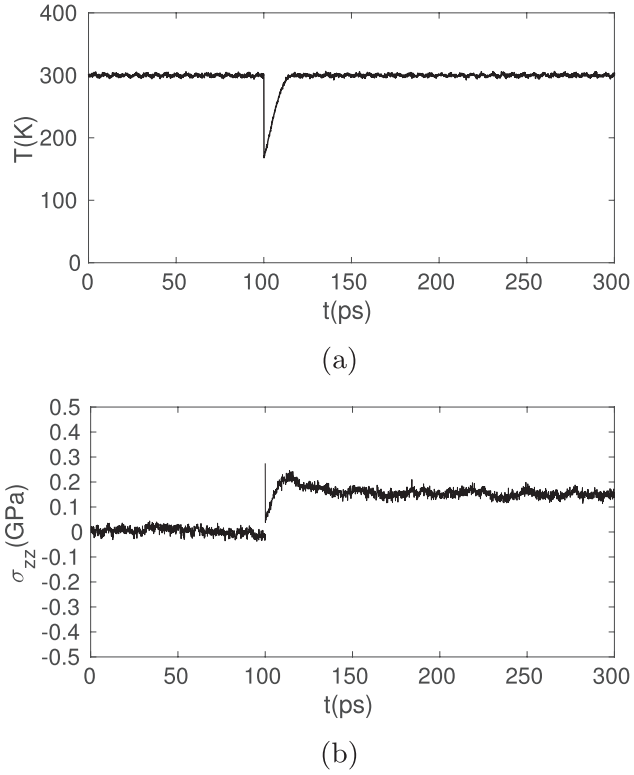


Figure 5. Temperature (a) and stress (b) equilibrium of MD simulations for 12 layers hBN model at 300 K.

accurately, compared to the other potentials. Note that the experimental value of c_{44} may be artificially high. This can be attributed to the use of pyrolytic samples [15], which generally have some covalent bonding between layers. These covalent bonds stiffen the structure, whereas our model assumes a perfect crystal.

3.4. Thermal conductivity

The thermal conductivity is calculated in the out-of-plane direction for the three different potentials at five different temperatures in the interval from 200 K to 400 K. Temperature is plotted versus non-dimensional length ($z^* = z/L$) along the out-of-plane direction, z^* in figure 7 for the proposed LJ 6–12 potential at an average temperature of 200 K, 250 K, 300 K, 350 K and 400 K. Only half of the simulation box is considered since the system is symmetric in z dimension due to the nature of Muller–Plathe algorithm. Linear temperature profiles are obtained for all five different cases, allowing Fourier's law to be applied. The thermal conductivity calculation is repeated for different number of layers to determine if there is any size effect for the MD predictions. Results for all three potentials are presented for 6, 8, 10, 12, 14, and 16 layers in figure 8. The absence of information about the number of layers in experiments precludes us from making a detailed comparison of thermal conductivity for each number of layers; however, the thermal conductivity in MD tends to increase with number of layers up to 14 layers. This is attributed to increased phonon boundary scattering for small models. Since there appear to be no significant changes in thermal conductivity from 12 layers

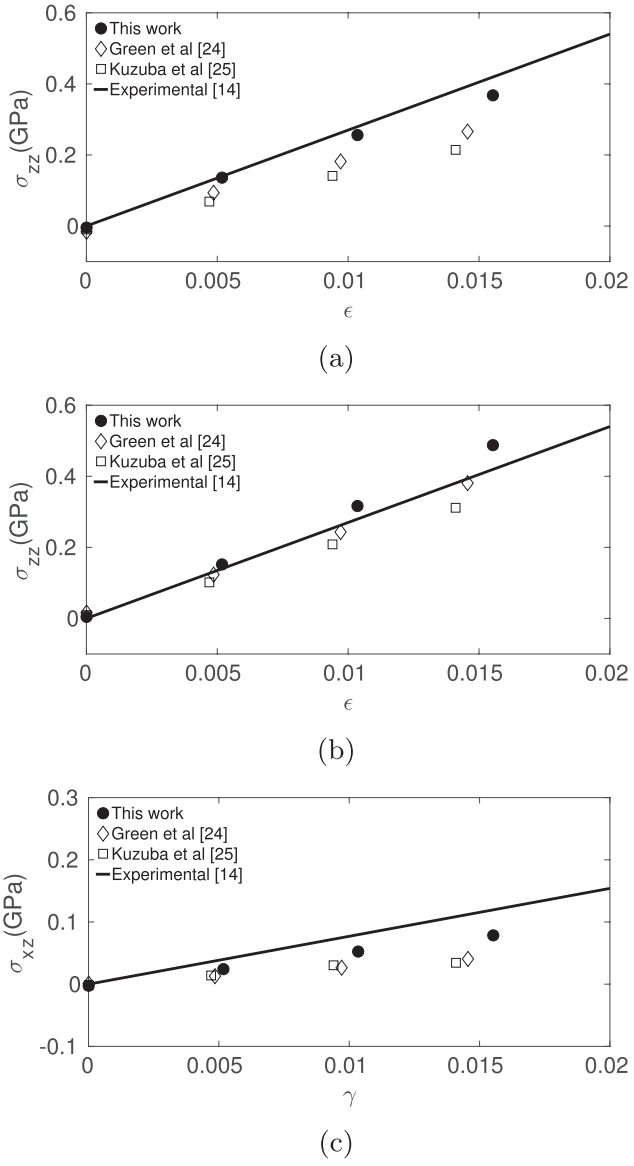


Figure 6. c_{33} in tension (a) in compression (b) and c_{44} (c) results of MD simulations using three different interlayer potentials.

to 16 layers, apart from fluctuations, the thermal conductivity of the 12 layer model is considered to be sufficient for the further analysis.

The thermal conductivity of MD simulations using different potentials for different temperatures is also considered with the results presented in figure 9. The proposed LJ 6–12 potential has the same (fluctuating) decreasing trend in thermal conductivity as the experimental studies [15]. The potentials of Green *et al* [24] and Kuzuba *et al* [25] fluctuate more and do not follow the experimental trend as well as the proposed potential. Moreover, the proposed potential predicts higher conductivities than the others, and its predictions are closer to experiments. More accurate representation of the transverse phonon modes may lead to this slight improvement of the thermal conductivity. All MD results are lower than the reported value of 2 W $m^{-1}K^{-1}$, [15]. This is reasonable because the experimental samples were pyrolytic with covalent bonds that could enhance the phonon transport along

Table 3. Elastic constants in GPa, and the percentage errors are presented in parenthesis.

	c_{33} (tens.)	c_{33} (comp.)	c_{44}
This work	23.9(11.5%)	31.2(15.6%)	5.25(31.9%)
Green *et al* [24]	19.3(28.6%)	24.98(7.5%)	2.73(64.6%)
Kuzuba *et al* [25]	15.83(41.4%)	21.56(20.1%)	2.67(65.4%)
Experiment [14]	27	27	7.7

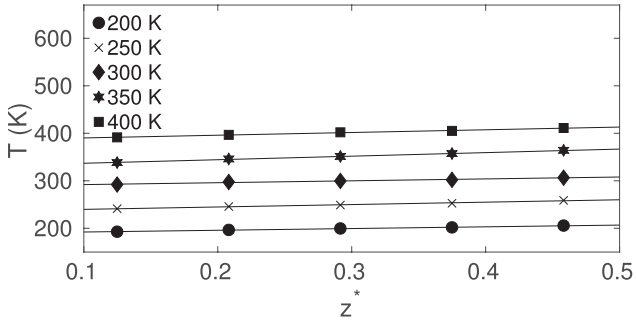


Figure 7. Temperature profile along out-of-plane direction of MLhBN.

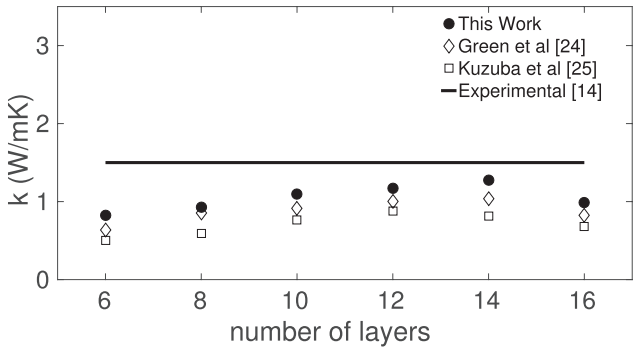


Figure 8. Out-of-plane thermal conductivity results for different potentials for different number of layers.

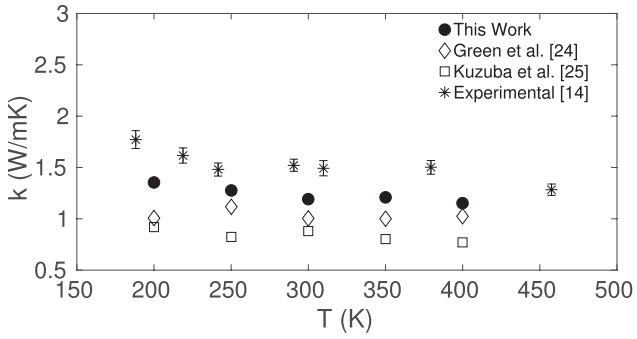


Figure 9. Out-of-plane thermal conductivity results of different potentials for different temperatures.

the out-of-plane direction. Hence, this difference in thermal conductivity is attributed to the ideal structure assumption in our models. The average errors with respect to the experimental thermal conductivity results in figures 8 and 9 are also presented table 4. It can be observed that the average error improvements of the proposed potential (with respect to the other potentials) are 11% and 23% for figure 8, and 7% and 27% for figure 9 [24] and [25].

Table 4. Average thermal conductivity percentage errors with respect to the experiments (for the results of figures 8 and 9) for different potentials.

Figure	This work	[24]	[25]
8	30.2	41.5	53
9	16	23.4	43

4. Conclusion

A new interlayer potential composed of Lennard-Jones 6–12 terms and a Coulombic term is developed for multi-layer hexagonal boron nitride. The derivation follows a similar fitting procedure to Kuzuba *et al* [25], but is calibrated with more recent experimental data for the hexagonal boron nitride and the rhombohedral boron nitride structures. The calibration is performed by a least squares minimization, and molecular dynamics simulations allow the performance of the proposed potential to be compared with two others with regard to interlayer spacing, elastic constants, and thermal conductivity. The proposed potential is found to predict the interlayer spacing more accurately, while errors for c_{33} predictons in compression are similar for all three potentials. The proposed potential again leads to the smallest error for c_{33} predictions in tension and for c_{44} predictions. More accurate elastic constants suggest that the proposed potential better reproduces phonon modes in the out-of-plane direction. The thermal conductivity is evaluated for the three potentials using the Muller–Plathe algorithm and the RNEMD method [33] as a function of temperature and the number of layers. The size effect is found not to be significant for systems with more than 10 layers. The thermal conductivity of the 12 layer model with the proposed potential decreases with increasing temperature, consistent with the increased phonon scattering that occurs in experiments. Overall, the proposed potential is found to more accurately predict properties such as density, elastic constants and thermal conductivity, and it is believed that this improvement will lead more accurate MD simulations of MLhBN.

Acknowledgment

Hakan Ertürk would like to thank The Scientific and Technological Research Council of Turkey (TUBITAK), for support under the grant 111M177 of the 1001 Program.

References

[1] Shi Y *et al* 2010 Synthesis of few-layer hexagonal boron nitride thin film by chemical vapor deposition *Nano Lett.* **10** 4134–9

[2] Golberg D, Bando Y, Huang Y, Terao T, Mitome M, Tang C and Zhi C 2010 Boron nitride nanotubes and nanosheets *Acs Nano* **4** 2979–93

[3] Haubner R, Wilhelm R and Lux B 2002 Chapter: high performance non-oxide ceramics II *Boron Nitrides—Properties, Synthesis and Applications* (*Structure and Bonding*) (Berlin: Springer)

[4] Humphrey W, Dalke A and Schulten K 1996 VMD—visual molecular dynamics *J. Mol. Graph.* **14** 33–8

[5] Duclaux L, Nysten B, Issi J P and Moore A W 1992 Structure and low-temperature thermal conductivity of pyrolytic boron nitride *Phys. Rev.* B **46** 3362

[6] Jo I, Pettes M T, Kim J, Watanabe K, Taniguchi T, Yao Z and Shi L 2013 Thermal conductivity and phonon transport in suspended few-layer hexagonal boron nitride *Nano Lett.* **13** 550–4

[7] Jauregui L A *et al* 2010 Thermal transport in graphene nanostructures: experiments and simulations *Ecs Trans.* **28** 73–83

[8] Khadem M H and Wemhoff A P 2013 Molecular dynamics predictions of the influence of graphite stacking arrangement on the thermal conductivity tensor *Chem. Phys. Lett.* **574** 78–82

[9] Ng T Y, Yeo J J and Liu Z S 2012 A molecular dynamics study of the thermal conductivity of graphene nanoribbons containing dispersed Stone–Thrower–Wales defects *Carbon* **50** 4887–93

[10] Singh S K, Neek-Amal M, Costamagna S and Peeters F M 2013 Thermomechanical properties of a single hexagonal boron nitride sheet *Phys. Rev.* B **87** 184106

[11] Boldrin L, Scarpa F, Chowdhury R and Adhikari S 2011 Effective mechanical properties of hexagonal boron nitride nanosheets *Nanotechnology* **22** 505702

[12] Mortazavi B and Rémond Y 2012 Investigation of tensile response and thermal conductivity of boron-nitride nanosheets using molecular dynamics simulations *Physica* E **44** 1846–52

[13] Sevik C, Kinaci A, Haskins J B and Çağın T 2011 Characterization of thermal transport in low-dimensional boron nitride nanostructures *Phys. Rev.* B **84** 085409

[14] Bosak A, Serrano J, Krisch Mi, Watanabe K, Taniguchi T and Kanda H 2006 Elasticity of hexagonal boron nitride: inelastic x-ray scattering measurements *Phys. Rev.* B **73** 041402

[15] Simpson A and Stuckes A D 1971 The thermal conductivity of highly oriented pyrolytic boron nitride *J. Phys. C: Solid State Phys.* **4** 1710

[16] Sanati M, Albers R C, Lookman T and Saxena A 2011 Elastic constants, phonon density of states, and thermal properties of uo 2 *Phys. Rev.* B **84** 014116

[17] Kong L T 2011 Phonon dispersion measured directly from molecular dynamics simulations *Comput. Phys. Commun.* **182** 2201–7

[18] Tersoff J 1989 Modeling solid-state chemistry: interatomic potentials for multicomponent systems *Phys. Rev.* B **39** 5566

[19] Albe K, Möller W and Heinig K H 1997 Computer simulation and boron nitride *Radiat. Eff. Defects Solids* **141** 85–97

[20] Lindsay L and Broido D A 2011 Enhanced thermal conductivity and isotope effect in single-layer hexagonal boron nitride *Phys. Rev.* B **84** 155421

[21] Marom N, Bernstein J, Garel J, Tkatchenko A, Joselevich E, Kronik L and Hod O 2010 Stacking and registry effects in layered materials: the case of hexagonal boron nitride *Phys. Rev. Lett.* **105** 046801

[22] Leven I, Azuri I, Kronik L and Hod O 2014 Inter-layer potential for hexagonal boron nitride *J. Chem. Phys.* **140** 104106

[23] Hickel T, Grabowski B, Körmann F and Neugebauer J 2011 Advancing dft to finite temperatures: methods and applications in steel design *Newsletter* **105** 22–50

[24] Green J F, Bolland T K and Bolland J W 1976 Theoretical elastic behavior for hexagonal boron nitride *J. Chem. Phys.* **64** 656–62

[25] Kuzuba T, Sato T, Ishii T and Arai T 1985 Interlayer binding of hexagonal boron nitride in the rigid-layer approximation *Phys. Rev.* B **32** 1230

[26] Bondi A 1964 van der Waals volumes and radii *J. Phys. Chem.* **68** 441–51

[27] Lewis G V and Catlow C R A 1985 Potential models for ionic oxides *J. Phys. C: Solid State Phys.* **18** 1149

[28] Ooi N, Rairkar A, Lindsley L and Adams J B 2005 Electronic structure and bonding in hexagonal boron nitride *J. Phys.: Condens. Matter* **18** 97

[29] Madelung O, Rossler U and Schulz M (ed) 2002 *Boron Nitride (BN), Properties of Rhombohedral BN* (*Landolt-Bornstein—Group 3 Condensed Matter* vol 41A1b) (Berlin: Springer) pp 1–11

[30] Qi Y and Hector L G 2007 Planar stacking effect on elastic stability of hexagonal boron nitride *Appl. Phys. Lett.* **90** 1922

[31] Anton H 2010 *Elementary Linear Algebra* (New York: Wiley)

[32] Plimpton S 1995 Fast parallel algorithms for short-range molecular dynamics *J. Comput. Phys.* **117** 1–19

[33] Müller-Plathe F 1997 A simple nonequilibrium molecular dynamics method for calculating the thermal conductivity *J. Chem. Phys.* **106** 6082–5